Deformation and Flow of Membrane into Tethers Extracted from Neuronal Growth Cones

Robert M. Hochmuth,* Jin-Yu Shao,* Jianwu Dai,‡ and Michael P. Sheetz‡
*Department of Mechanical Engineering and Materials Science and ‡Department of Cell Biology, Duke University, Durham, North Carolina 27708 USA

ABSTRACT Membrane tethers are extracted at constant velocity from neuronal growth cones using a force generated by a laser tweezers trap. A thermodynamic analysis shows that as the tether is extended, energy is stored in the tether as bending and adhesion energies and in the cell body as "nonlocal" bending. It is postulated that energy is dissipated by three viscous mechanisms including membrane flow, slip between the two monolayers that form the bilayer, and slip between membrane and cytoskeleton. The analysis predicts and the experiments show a linear relation between tether force and tether velocity. Calculations based on the analytical results and the experimental measurements of a tether radius of ~0.2 μm and a tether force at zero velocity of ~8 pN give a bending modulus for the tether of 2.7×10^{-19} N·m and an extraordinarily small "apparent surface tension" in the growth cone of 0.003 mN/m, where the apparent surface tension is the sum of the far-field, in-plane tension and the energy of adhesion. Treatments with cytochalasin B and D, ethanol, and nocodazole affect the apparent surface tension but not bending. ATP depletion affects neither, whereas large concentrations of DMSO affect both. Under conditions of flow, data are presented to show that the dominant viscous mechanism comes from the slip that occurs when the membrane flows over the cytoskeleton. ATP depletion and the treatment with DMSO cause a dramatic drop in the effective viscosity. If it is postulated that the slip between membrane and cytoskeleton occurs in a film of water, then this water film has a mean thickness of only ~10 Å.

INTRODUCTION

Highly curved membrane cylinders, called "tethers" (Fig. 1), are readily extracted from man-made vesicles (Waugh, 1982) and from living cells, including red cells (Hochmuth et al., 1973, 1982) and neuronal growth cones (Dai and Sheetz, 1995a). Tether diameters can be smaller than 10 nm (Hochmuth et. al, 1983) and larger than 100 nm (Dai and Sheetz, 1995a) and are observed to decrease in value as the tension exerted on the membrane in the "far field," far from the tether, is increased (Hochmuth et al., 1983; Evans and Yeung, 1994). When tethers are extracted from neuronal growth cones (Dai and Sheetz, 1995a) and from vesicles while the far-field tension is held constant (Evans and Yeung, 1994), the force on the tether increases linearly with the velocity of extraction, which indicates that the viscous resistance in this process is linear, or "Newtonian." However, even though the force increases with velocity, the diameter of the tether remains constant for tethers extracted both from simple vesicles (Evans and Yeung, 1994) and from neuronal growth cones.

An analysis of the tether-formation process is important for several reasons. First, it allows the bending rigidity of highly curved membranes to be calculated. Second, it leads to a calculation of the apparent surface tension that exists in the membrane. The apparent surface tension, in turn, becomes a sensitive measure of secretion because when secreting cells are stimulated a significant decrease in apparent surface tension is observed (Dai and Sheetz, 1995b). Third, an analysis allows the identification of the kinds of dissipation that occur when a tether is extracted from a cell at a finite rate. In general, a study of tethers leads to a further understanding of the membrane–cytoskeleton interface and is particularly relevant to the processes of secretion and signaling.

Here a basic thermodynamic (energy) analysis of the tether-formation process is presented and then applied to experimental studies of the formation of tethers from neuronal growth cones. The analysis, based on a simple geometric system in which a cylindrical tether is drawn from an axisymmetric membrane disk, is designed to reveal the essential physical and mathematical features of both static and dynamic tether-formation processes without the need to appeal to complex mathematics. Whenever possible, the results will be compared with the results of others to establish the validity of this approach. A result of the analysis allows the apparent surface tension, which is the sum of the in-plane, far-field tension and the energy of adhesion between membrane and cytoskeleton, to be calculated. Another result reveals a simple relationship between the force on a tether at a given velocity and the viscous resistance that occurs when a membrane slips over the underlying cytoskeleton. This result leads to the calculation of a value for the viscous resistance and an estimate of the thickness of a lubricating film of water that is postulated to exist between the membrane and the cytoskeleton.

Received for publication 30 June 1995 and in final form 13 October 1995.
Address reprint requests to Dr. Robert M. Hochmuth, Department of Mechanical Engineering and Materials Science, Box 90300, Duke University, Durham, NC 27708-0300. Tel: (919) 660-5307; Fax: (919) 660-8963; E-mail: hochmuth@acpub.duke.edu.

0006-3495/96/01/358/12 $2.00

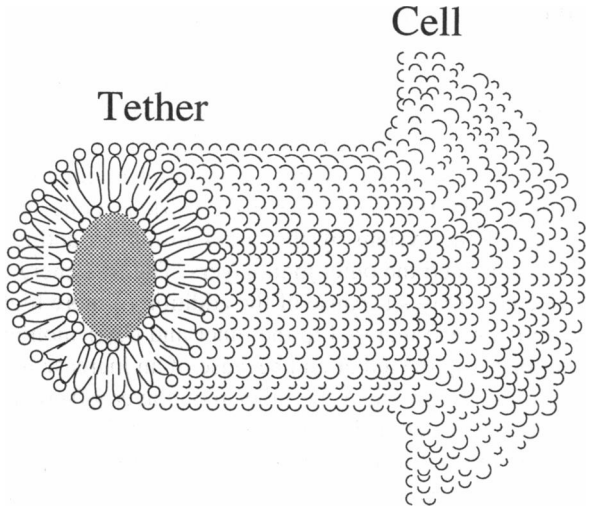

FIGURE 1 Membrane tether showing the lipid bilayer. The cylindrical tether is extracted from the cell body by pulling on the tether with a constant velocity. The cell body is modeled as a flat disk whose plane is perpendicular to the axis of the tether.

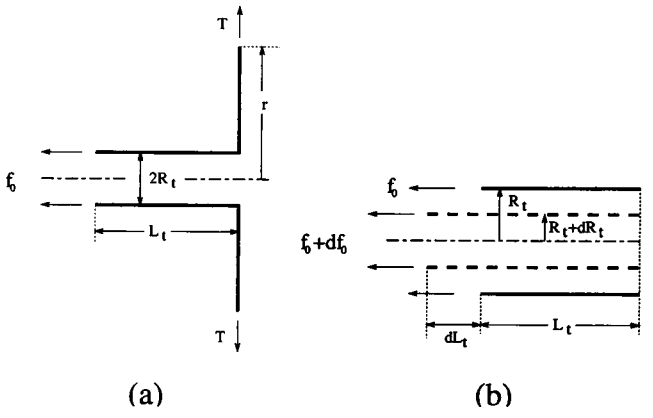

FIGURE 2 (*a*) Model of a simple monolayer as a membrane disk of radius r and a tether of radius R_t and length L_t. The far-field stress resultant or "tension" in the membrane is T, and the axial force acting on the tether is f_0. (*b*) A tether with a fixed area that decreases in radius by an amount dR_t and increases in length by dL_t because of a small increment df_0 in the axial force.

THERMODYNAMIC EQUILIBRIUM

Simple monolayer

The combined first and second laws of thermodynamics state that the reversible, isothermal work on the boundary of a system dW (work on a system is taken as positive) equals the change in the Helmholtz free energy dE of the system for quasi-static processes. Here the system is the simple monolayer shown in Fig. 2a. The work on the system is done by the tether force at zero velocity f_0 and the far-field, in-plane tension T when the tether is displaced a small distance dL_t and the far-field, in-plane tension is displaced a distance dr:

$$dW = f_0 dL_t + 2\pi r T dr = (f_0 - 2\pi R_t T) dL_t, \qquad (1)$$

where the term $2\pi r dr$ in Eq. 1 is eliminated because of conservation of area: $2\pi r dr = -2\pi R_t dL_t$. The increase in energy of the system when forming a tether comes from two sources: (1) an increase in bending energy owing to the movement of membrane with no curvature from the disklike cell body to the cylindrical tether with a constant curvature c and (2) the separation of the membrane from the cytoskeleton where there is a chemical affinity or free energy of adhesion γ between membrane and cytoskeleton. In this case the increase in free energy of the system is

$$dE = \frac{B}{2} c^2 dA + \gamma dA = \left(\frac{\pi B}{R_t} + 2\pi R_t \gamma\right) dL_t, \qquad (2)$$

where $c = 1/R_t$, $dA = 2\pi R_t dL_t$, γ is the energy of adhesion, and B is the bending modulus for a simple monolayer.

In Eq. 2 and the equations to follow, the stress-free state is a flat surface, which means that the spontaneous curvature is assumed to be zero. Because most of the surface of the neuronal growth cone is flat or nearly so, a spontaneous curvature would produce a tension gradient from the inner to the outer surface, causing a transfer of lipids and decreasing the spontaneous curvature toward zero. In addition, calculations of the bending modulus for neuronal growth cones with these equations give a value for B that is close to those for large lipid vesicles for which the spontaneous curvature is known to be negligible.

The sharp corners shown in Fig. 2 and the following figures are a convenient abstraction and are not meant to represent the actual situation. Nevertheless, the shape is not important as long as it does not change when incremental or steady-state work is performed at the boundary of the system. As we will show, the tether radius does not change during both static and dynamic tether-formation processes. In addition, the shape of the transition between cell body and tether does not appear to change, and therefore no additional energy will be stored there. Additional energy is stored only as surface energy and as bending energy in the elongating tether in accordance with Eq. 2.

When Eqs. 1 and 2 are equated, a fundamental equation is obtained that relates the static tether force f_0 to the apparent surface tension $T + \gamma$ and the bending modulus B:

$$f_0 = 2\pi R_t (T + \gamma) + \frac{\pi B}{R_t}. \qquad (3)$$

A similar relation was given first by Bo and Waugh (1989) for the case in which a tether is drawn from a vesicle aspirated into a micropipet, and thus in their case $\gamma = 0$ and T was replaced by the pipet suction pressure according to the law of Laplace for an aspirated vesicle. Equation 3 shows for a simple membrane tether that the force on the tether has two components: one that is due to the apparent surface tension and another that is due to the bending of the membrane. Another independent relation between the tether force and the bending of a tether can be obtained by considering the work on an isolated tether with a constant

membrane surface area (Fig. 2 *b*). The deformation is produced by a small increment in the static force on the tether f_0. Inasmuch as the area remains constant, the change in the free energy comes only from a change in the curvature:

$$E - E_0 = \frac{B}{2}c^2A + \gamma A \Rightarrow dE = BAcdc = -\frac{2\pi BL_t}{R_t^2}dR_t, \quad (4)$$

where E_0 is the reference energy corresponding to the state where $c = 0$ and $\gamma = 0$. Equating the work at the boundary, $f_0 dL_t$, to the change in the free energy of the tether, Eq. 4, and using the relationship for constant surface area A ($2\pi R_t L_t = A \Rightarrow R_t dL_t = -L_t dR_t$) gives

$$f_0 = \frac{2\pi B}{R_t}. \quad (5)$$

Equation 5 was first given by Waugh and Hochmuth (1987) from an analysis of the static equilibrium of a tether as a thick, hollow, liquid-membrane cylinder. Equation 5 shows that, for a simple monolayer, each of the two terms in Eq. 3—one caused by apparent surface tension and the other by bending—contributes equally to the total force on the tether.

Equations 3 and 5 can be combined to eliminate any one of the variables—f_0, R_t, T—in favor of the other two. These equations also can be combined to eliminate the term for the bending modulus. Nevertheless, none of these simplifications will be done at this point because, strictly speaking, both equations are incorrect in that they fail to take account of the fact that all biological membranes are bilayers made up of two monolayers. The monolayers are free to slip past each other (Evans and Yeung, 1994) and, in doing so, they create, for a closed (fixed mass) membrane system, an induced bending, often referred to as a nonlocal bending or a nonlocal curvature elasticity (Evans, 1980).

Bilayer

A bilayer that is drawn from a membrane disk onto a cylindrical tether is shown in Fig. 3 *a*. Here the stress resultants in the far field on the inner and outer (external) monolayers are T_i and T_e, the far-field radii are r_i and r_e, the axial stress resultants acting on the tether are T_{zi} and T_{ze}, the inner and outer tether radii are R_{ti} and R_{te}, and the mean tether radius is $R_t = R_{ti} + (h/2) = R_{te} - (h/2)$. The distance between the surfaces on which the stress resultants act is h. Its value will be of the order of the thickness of the membrane bilayer. As more membrane material is drawn onto the tether from the membrane disk, work is done at the boundary of the system by the stress resultants acting on both the inner and the outer monolayers. The free energy of the system increases because of the addition of more highly curved membrane material to the inner and outer monolayers that make up the tether and because of an increase in the energy of adhesion when the inner monolayer is separated from the cytoskeleton. Because the areas of the inner and outer membrane surfaces will remain essentially constant for a small displacement dL_t of the tether, $r_e dr_e = R_{te}dL_t$ and $r_i dr_i = R_{ti}dL_t$. Equating the work at the boundary of the system to the change in the free energy and using the constant area relationships to express the result in terms of dL_t gives, after dL_t is canceled from the result,

$$f_0 = 2\pi R_{te}T_e + 2\pi R_{ti}T_i + 2\pi R_{ti}\gamma + \frac{\pi B_e}{R_{te}} + \frac{\pi B_i}{R_{ti}}, \quad (6)$$

where in Eq. 6 the sum of the inner and outer axial stress resultants times their respective circumferences is replaced by the net static force f_0 on the tether and B_e and B_i denote the bending moduli for the outer and inner monolayers.

The overall tension in the far field is the sum of the tensions acting on the individual monolayers:

$$T = T_e + T_i. \quad (7)$$

When Eq. 7 is substituted into Eq. 6 along with $R_t = R_{ti} + (h/2) = R_{te} - (h/2)$ and the assumption made that $B_e = B_i = B/2$, where B is the overall bending modulus for the bilayer membrane, then the following is obtained:

$$f_0 = 2\pi R_t(T + \gamma) + \frac{\pi B}{R_t} + \pi h(T_e - T_i) - \pi h\gamma, \quad (8)$$

where the higher-order term, which is of the order of $(h/2R_t)^2$, is neglected.

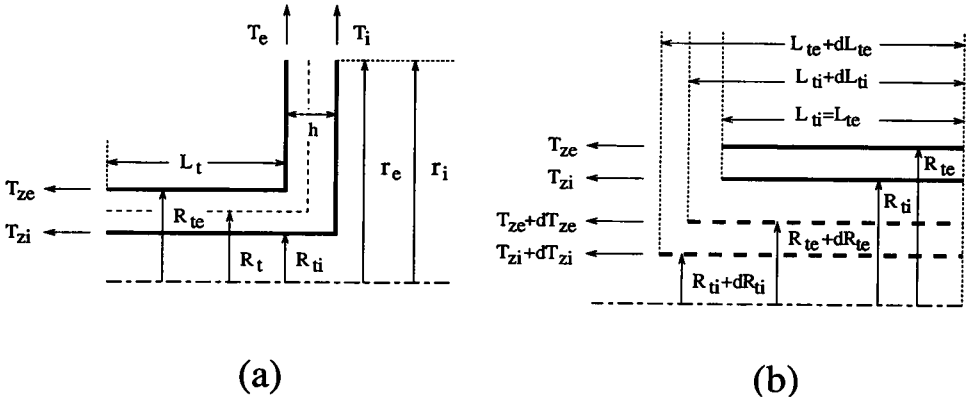

FIGURE 3 (*a*) Model of a bilayer as two monolayers separated by a distance h. The subscripts i and e stand for "inner" and "outer" (external). All variables, minus the subscripts, are defined in Fig. 2 *a*. (b) Bilayer made of two monolayers. The area of each monolayer remains fixed as the bilayer is deformed by small increments in the axial stress resultants. Note that the change in length of the inner monolayer, dL_{ti}, is greater than that for the outer (external) monolayer, dL_{te}.

Now the "mistake" in Eq. 3 can be seen. Equation 3 ignores the fact that the membrane has two monolayers that are free to slip, one relative to the other, and when this happens the tensions in the individual monolayers can change because of the expansion of the outer monolayer and the compression of the inner monolayer as the two layers are drawn together into the highly curved tether. (The outer monolayer on the tether has a larger area than the inner monolayer.) These changes in the monolayer areas can occur even when the overall tension (and the overall area) in the bilayer membrane remains constant. The term $\pi h(T_e - T_i)$ in Eq. 8 can be thought of as an induced bending moment that comes from the differential expansion of the outer monolayer relative to the compression of the inner monolayer. Because this differential expansion and compression occur over the entire membrane surface for a closed system with freely slipping monolayers, the term $\pi h(T_e - T_i)$ represents a "nonlocal curvature elasticity." Expressions for the nonlocal bending, which depend directly and linearly on the tether length and inversely on the total membrane surface area, are given by Waugh et al. (1992) and Evans and Yeung (1994). These expressions are based on the assumptions that the tension in a monolayer is linearly related to the change in area of the monolayer and that the expansion/compression moduli for the inner and outer monolayers are equal and exactly half the value of the expansion modulus for a bilayer.

The last term in Eq. 8, $-\pi h\gamma$, comes from the fact that only the inner membrane surface can adhere to the cytoskeleton. Only if $h \ll R_t$ can this term be neglected.

A relation between the tether force and the tether radius for two freely slipping monolayers that is independent of the relation given by Eq. 8 can be developed, just as was done for a single monolayer (Eq. 5), by considering the work on an isolated tether with constant monolayer surface areas. For constant areas, the relations between the changes in the outer and inner tether lengths and the outer and inner tether radii are

$$dL_{te} = -\frac{L_{te}}{R_t + (h/2)}\,dR_t, \qquad dL_{ti} = -\frac{L_{ti}}{R_t - (h/2)}\,dR_t, \tag{9}$$

where the tether lengths, L_{te} and L_{ti}, in Eq. 9 are evaluated at the initial state of deformation when $L_{te} = L_{ti}$. Now, refer to Fig. 3 *b* and equate the work at the boundary to the change in free energy of the tether that is due to the increase in curvature of each of the monolayers and then use Eq. 9 to obtain an expression that is homogeneous in dR_t. Here the goal is to obtain an expression analogous to Eq. 5 but for freely slipping monolayers. Thus, the forces acting on the inner and outer monolayers are substituted for the inner and outer axial tensions times their respective circumferences. The result is

$$\frac{f_e}{R_{te}} + \frac{f_i}{R_{ti}} = \frac{2\pi B_e}{R_{te}^2} + \frac{2\pi B_i}{R_{ti}^2}. \tag{10}$$

Substituting the expressions for the inner and outer tether radii, $R_t = R_{ti} + (h/2) = R_{te} - (h/2)$, into Eq. 10, assuming that $B_e = B_i = B/2$, and neglecting the higher-order term, $(h/2R_t)^2$, gives

$$f_0 = \frac{2\pi B}{R_t} + (f_e - f_i)\frac{h}{2R_t}. \tag{11}$$

Equation 3 can be used to evaluate f_e and f_i because they represent forces on monolayers (note that $\gamma = 0$ for f_e). Thus, when Eq. 3 is substituted into Eq. 11 and higher-order terms are neglected, the following is obtained:

$$f_0 = \frac{2\pi B}{R_t} + \pi h(T_e - T_i) - \pi h\gamma. \tag{12}$$

The "mistake" in Eq. 5 can be seen by comparing Eq. 5 with Eq. 12, just as the mistake in Eq. 3 was seen by comparing Eq. 3 with Eq. 8.

Tether radius

Although both Eqs. 8 and 12 depend on the induced bending moment, which in turn depends on the tether length, the difference of the two equations is independent of tether length. Thus, when Eq. 12 is subtracted from Eq. 8, the following important result is immediately obtained:

$$T + \gamma = \frac{B}{2R_t^2} \Rightarrow R_t^2 = \frac{B}{2(T + \gamma)}. \tag{13}$$

This expression, obtained originally by Waugh et al. (1992) and Evans and Yeung (1994) for the case where $\gamma = 0$, shows that the tether radius does not depend on the length of the tether because the induced bending terms in Eqs. 8 and 12 cancel each other when they are subtracted. (Of course, Eq. 13 could be obtained by subtracting Eq. 5 from Eq. 3, without appreciating the fact that Eq. 13 is true for both a simple monolayer and a bilayer.) The tether radius depends only on the bending modulus for the tether and the apparent surface tension $T + \gamma$.

VISCOUS FLOW

When a tether is extracted from a cell or vesicle at a finite, nonequilibrium rate, the rate of work at the boundary of the system, $\dot{W}$, must exceed the rate of change in the bending and adhesion energies of the system, $\dot{E}_b + \dot{E}_\gamma$. This additional work goes into overcoming the viscous resistance or the viscous dissipation within the system. (Note that the work at the boundary of the system includes the (positive) work on the tether, the (negative) work in the far field on the monolayers, and the (negative) work done to overcome the viscous resistance of the cytoskeleton.) For an isothermal system, the viscous dissipation generates heat that is lost to the surroundings. Thus, the first law of thermodynamics becomes

$$\dot{W} = \dot{E}_b + \dot{E}_\gamma - \dot{Q} = \dot{E}_b + \dot{E}_\gamma + \dot{I}, \tag{14}$$

where $-\dot{Q}$ represents the heat lost to the surroundings. This heat is generated by viscous dissipation, denoted by $\dot{I}$. The dissipation in the system is given as the double-dot product of the stress tensor $\underline{\underline{\tau}}$ and the velocity gradient $\nabla \boldsymbol{v}$:

$$\dot{I} = \iiint (\underline{\underline{\tau}} : \nabla \boldsymbol{v})\, dV = \iiint \eta \Phi\, dV, \qquad (15)$$

where η is a viscosity and Φ is the dissipation function. Expressions for these terms in the appropriate coordinate system (cylindrical in this case) are given in Bird et al. (1960).

A simple disklike cell body (Fig. 4) is chosen to analyze the flow of membrane from cell body to tether. The velocity of the tether is V_t and, because the surface areas of the inner and outer monolayers remain constant as they flow from cell body to tether, the inner (v_{ri}) and outer (v_{re}) monolayer velocities at any radial position r are

$$v_{ri} = \frac{-R_{ti}V_t}{r}, \qquad v_{re} = \frac{-R_{te}V_t}{r}. \qquad (16)$$

It is postulated that there are three sources of viscous resistance, as shown in Fig. 4. First there is a viscous drag between the inner monolayer and the cytoskeleton. (There also is a viscous drag between the outer monolayer and the extracellular fluid. However, this viscous drag is likely to be much less than the drag of the cytoskeleton.) This viscous drag of the cytoskeleton causes a shear stress to be exerted on the monolayer:

$$\tau_{sc} = -\eta_{sc} v_{ri}, \qquad (17)$$

where η_{sc} is a slip viscosity and the subscripts *sc* stand for "slip" and "cytoskeleton." The rate of (negative) work that the system does on the cytoskeleton because of this viscous drag is

$$\dot{W}_{sc} = \int_{R_{ti}}^{R_o} \tau_{sc} 2\pi r\, dr \cdot v_{ri} = -\int_{R_{ti}}^{R_o} \eta_{sc} v_{ri}^2 2\pi r\, dr. \qquad (18)$$

When Eq. 16 is substituted into Eq. 18 and the integration performed, the result is

$$\dot{W}_{sc} = -2\pi\eta_{sc} R_t^2 V_t^2 \ln \frac{R_o}{R_t}, \qquad (19)$$

where the mean tether radius has been substituted for the inner tether radius ($R_{ti} = R_t - h/2 \approx R_t$) and R_o is some characteristic far-field radius for the neuronal growth cone.

In addition to this viscous drag at the boundary of the system, there is a viscous slip between the two halves of the bilayer (Evans and Yeung, 1994):

$$\tau_{si} = \eta_{si}(v_{re} - v_{ri}), \qquad (20)$$

where the subscripts *si* stand for "slip" and "interbilayer." When Eq. 15 is rewritten for this special case of interbilayer slip and Eqs. 20 and 16 are substituted into Eq. 15 with $dV = 2\pi r h dr$, the result is

$$\dot{I}_{si} = \int_{R_t}^{R_o} \eta_{si}(v_{re} - v_{ri})^2 2\pi r\, dr = \int_{R_t}^{R_o} \eta_{si} \frac{h^2 V_t^2}{r^2} 2\pi r\, dr = 2\pi\eta_{si} h^2 V_t^2 \ln \frac{R_o}{R_t}. \qquad (21)$$

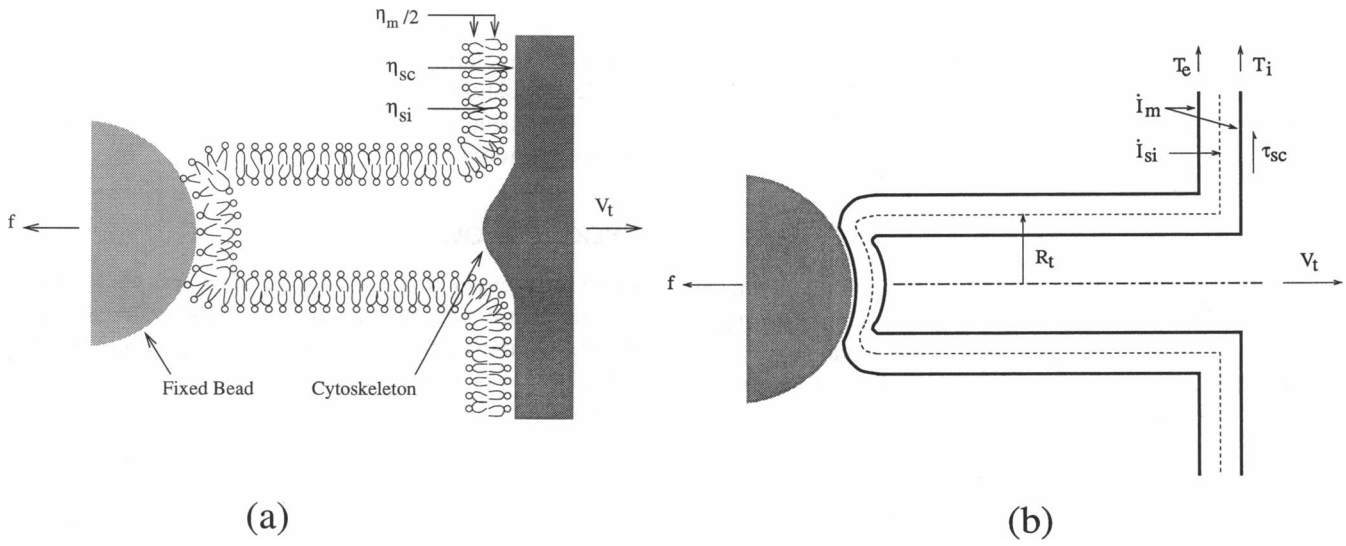

FIGURE 4 (*a*) Schematic of a tether being pulled off a cytoskeleton at a velocity V_t. The tether is attached to a bead held in place with a force f created by an optical laser trap or "tweezers." Three sources of dissipation or viscosities are postulated: one that is due to the surface viscosity in each of the monolayers, $\eta_m/2$, one that is due to the viscous slip between each of the monolayers, η_{si}, and one that is due to the viscous slip of the (inner monolayer) membrane over the cytoskeleton, η_{sc}. The subscript *m* stands for "membrane," *s* stands for "slip," *i* stands for "interbilayer," and *c* stands for "cytoskeleton." (*b*) Line drawing of (a). The rate of dissipation in the membrane is $\dot{I}_m$, and that which is due to the slip between the monolayers is $\dot{I}_{si}$. The shear stress exerted on the inner membrane as it is dragged over the cytoskeleton is τ_{sc}.

Finally, it is postulated that the membrane has a surface viscosity (Hochmuth and Evans, 1982) that causes a surface-stress resultant because of the extensional flow of membrane from cell body to tether:

$$T_{re} = T_e + 2\eta_e \frac{\partial v_{re}}{\partial r}, \qquad T_{ri} = T_i + 2\eta_i \frac{\partial v_{ri}}{\partial r}, \quad (22)$$

where η_e and η_i are the outer (external) and inner membrane surface viscosities. For this case the dissipation function (Eq. 15) can be evaluated for both inner and outer monolayers by using results given by Bird et al. (1960):

$$\dot{I}_m = \eta_e \int_{R_{ti}}^{R_o} 2\left[\left(\frac{\partial v_{re}}{\partial r}\right)^2 + \left(\frac{v_{re}}{r}\right)^2\right] 2\pi r\, dr + \eta_i \int_{R_{ti}}^{R_o} 2\left[\left(\frac{\partial v_{ri}}{\partial r}\right)^2 + \left(\frac{v_{ri}}{r}\right)^2\right] 2\pi r\, dr, \quad (23)$$

where the three-dimensional viscosity times the differential volume in Eq. 15, ηdV, has been replaced by a (two-dimensional) surface viscosity times a differential surface area, $\eta_e 2\pi r dr$ and $\eta_i 2\pi r dr$. The substitution of Eq. 16 into Eq. 23 and the subsequent integration gives

$$\dot{I}_m = 4\pi\eta_m V_t^2 \quad (24)$$

where terms of the order of $(R_t/R_o)^2$ have been neglected and where $\eta_m = \eta_e + \eta_i$.

The rate of work at the boundary of the system shown in Fig. 4 can be equated to the rate of dissipation and the rate of change in the energy of the system that are due to bending and adhesion:

$$f \cdot V_t + \dot{W}_{sc} + T_e 2\pi r v_{re} + T_i 2\pi r v_{ri} = \left(\frac{\pi B_e}{R_{te}} + \frac{\pi B_i}{R_{ti}} + 2\pi R_{ti}\gamma\right) V_t + \dot{I}_m + \dot{I}_{si}. \quad (25)$$

Equation 16 can be used to eliminate rv_{re} and rv_{ri} in Eq. 25. In addition, all the appropriate equations (Eqs. 19, 21, and 24) can be substituted into Eq. 25 and the inner and outer tether radii replaced by $R_{ti} = R_t - h/2$ and $R_{te} = R_t + h/2$. Finally, when the tether velocity is canceled from both sides of the equation and higher-order terms are neglected, the following general result is obtained:

$$f = 2\pi R_t(T + \gamma) + \pi B/R_t + \pi h(T_e - T_i) - \pi h\gamma + 2\pi V_t[2\eta_m + \eta_{si}h^2\ln(R_o/R_t) + \eta_{sc}R_t^2\ln(R_o/R_t)]. \quad (26)$$

Note that the nonviscous part of Eq. 26 (i.e., the part not multiplied by the tether velocity V_t) is identical to Eq. 8. This gives the tether force at zero velocity, f_0.

The first viscous term in Eq. 26, which accounts for the membrane surface viscosity, η_m, has been derived by Hochmuth and Evans (1982). The second term, which accounts for the slip viscosity between the two monolayers, η_{si}, has been derived by Evans and Yeung (1994). Both of these derivations were based on the equations of membrane mechanics. The third term, which accounts for the slip viscosity between membrane and cytoskeleton, η_{sc}, is new. Note that this term has a larger scale factor—the square of the tether radius—than the term that accounts for the slip viscosity between the monolayers where the scale factor is the square of the effective membrane thickness. Thus, even if the values for the two slip viscosities are equal, the drag from the cytoskeleton will dominate that from interbilayer slip because of the larger scale factor.

EXTRACTION OF TETHERS FROM NEURONAL GROWTH CONES

Neuronal growth cones from chick embryos were cultured and prepared for study as described by Dai and Sheetz (1995a). Latex beads (Duke Scientific, Palo Alto, CA) coated with rat IgG (Sigma, St. Louis, MO) were allowed to adhere to growth cones that, in turn, were adhering to a cover slip in a chamber mounted upon a microscope stage. The latex beads were held in a laser-tweezers trap, and the stage was moved with a piezoceramic driver (Wye Creek Instruments, Frederick, MD) at a constant velocity away from the bead being held in the laser trap, creating a tether. The movement of the bead in the trap is proportional to the force exerted on the bead by the tether. The force was calibrated with the method of Kuo and Sheetz (1993), and the nanometer displacements of the bead were tracked (Gelles et al., 1988). The results of the measurements of tether force versus velocity are shown in Fig. 5a. Here 57 data points are plotted for velocities as large as 18.5 μm/s. This plot includes 26 data points from the work of Dai and Sheetz (1995a) in which the maximum velocity was ~6 μm/s. In that paper the slope, from a straight-line fit, of the force-versus-velocity data was 1.51 pN · s/μm, whereas here it is somewhat less and has a value of 0.861 pN · s/μm. The tether force at zero velocity, f_0, is ~8.2 pN in Fig. 5 *a* and 6.7 pN in the work of Dai and Sheetz (1995a). Measurements made at negative velocities (data not shown) essentially fell on the extrapolation of the straight line of the curve shown in Fig. 5 *a*. The extrapolation to zero force gives a negative velocity between 10 and 12 μm/s, which is the velocity observed (but not measured precisely) when the bead is released from the trap. (The force produced by the Stokes drag on a 0.5-μm-diameter sphere at these velocities will be less than 0.1 pN.) Finally, when tethers from neuronal growth cones are extracted at constant velocity and the tether is suddenly stopped, the tether force at zero velocity at different tether lengths can be measured. No correlation of this force with tether length is observed (data not shown). That is, the tether force at zero velocity was not observed to increase (or decrease) with tether length. This means that the induced bending term is not important when tethers are extracted from neuronal growth cones from chick embryos. For tethers from neuronal growth cones, $2R_t$ = 410 nm (shown below). Inasmuch as h is generally 4 nm, $2R_t \gg h$. Consequently, $2\pi R_t T = 2\pi R_t(T_e + T_i) \gg$

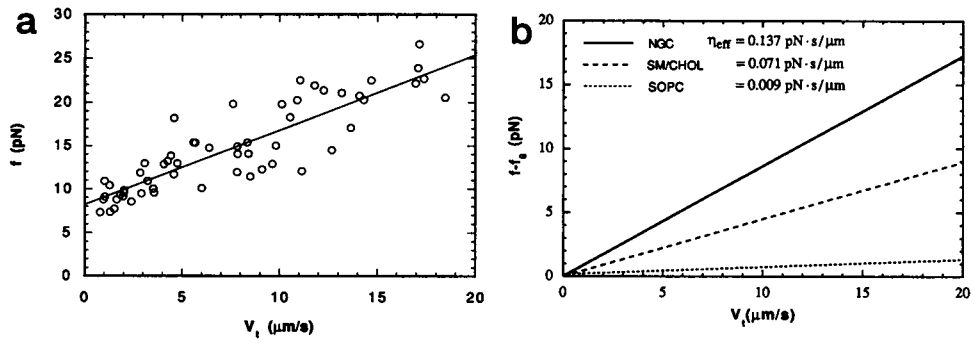

FIGURE 5 (*a*) Measured force versus velocity for 57 tethers extracted from neuronal growth cones. Twenty-six of these points, all at velocities of less than 6 μm/s, are from Dai and Sheetz (1995a). (*b*) Results from (*a*) for neuronal growth cones (NGC) and from Evans and Yeung (1994) and Yeung (1994) for tethers extracted from single-walled vesicles made from simple phospholipid bilayers of sphingomyelin/cholesterol (SM/CHOL) and 1-stearoyl-2-oleoyl-*sn*-glycero-3-phosphocholine (SOPC). The effective viscosity, η_{eff}, is defined by Eq. 29b in the text and is simply the slope of the line divided by 2π.

$\pi h(T_e - T_i)$ and $2\pi R_t\gamma \gg \pi h\gamma$. This mathematically explains why the induced bending term and the $\pi h\gamma$ term are not important either in Eq. 26 or in the equations for the force on a static tether (Eqs. 8 and 12).

In Fig. 5 *b* the straight-line fit for neuronal growth cones is compared with the results from Evans and Yeung (1994) and Yeung (1994) for single bilayer vesicles made from the simple phospholipid SOPC and from a 1:1 mixture of bovine brain sphingomyelin and cholesterol (SM/CHOL). Note from the figure that the tether force relative to the tether force at zero velocity, $f - f_0$, is plotted on the ordinate. Also, it is noted that the data of Evans and Young had virtually no scatter.

To measure the diameter of a tether, orthogonal scans across the differential interference contrast images of both the tether and the axon of the neuronal growth cone were made, and the relative intensities were determined (Schnapp et al., 1988). After the diameter of the axon was measured by the method of Gelles et al. (1988), the diameter of the tether was calculated simply by multiplying the diameter of the axon by the square root of the ratio of the intensity of the growth cone to that of the axon. (The intensity should be related to the square of the diameter.) The diameter of the tether was calculated to be ~400 nm, and there was no detectable change in tether diameter with increasing velocity, so the diameter remained constant. Results from 10 experiments are shown in Fig. 6. As can be seen, the average tether diameter is 410 nm. This measurement of diameter was validated by using latex beads 500 nm (0.5 μm) in diameter as a standard and measuring them according to the method of Gelles et al. (1988). Then from a video tape the diameter of the tether was measured and compared with the standard bead value. The same value for the tether diameter was obtained with the bead as a reference, which gives confidence in the method of measurement.

Tether force at zero velocity

The experimental evidence that the tether radius remains constant during the tether-formation process means that the static equilibrium terms in Eq. 26, other than the induced-moment term and the $\pi h\gamma$ term, can be replaced by a constant force term f_0:

$$f_0 = 2\pi R_t(T + \gamma) + \pi B/R_t, \tag{27a}$$

where the induced moment and the $\pi h\gamma$ terms are neglected for the reasons given above. Because of the unique relation between tether radius and the far-field membrane tension (Eq. 13), Eq. 27a can be written in three other ways:

$$f_0 = \frac{2\pi B}{R_t}, \tag{27b}$$

$$f_0 = 4\pi R_t(T + \gamma), \tag{27c}$$

$$f_0 = 2\pi\sqrt{2B(T + \gamma)}. \tag{27d}$$

Because the tether force at zero velocity for neuronal growth cones was not observed to depend in any way on tether length, Eqs. 27 are independent of tether length. Note that this is true only for this particular experimental system. In general, the tether force at zero velocity will depend on

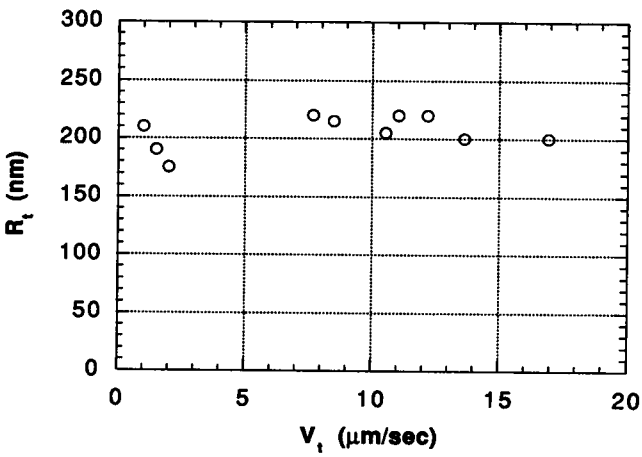

FIGURE 6 Tether radius at different tether velocities. The method of measurement is described in the text. Note the constant radius of ~210 nm.

tether length (Waugh et al., 1992; Evans and Yeung, 1994). It is only the tether radius, at a fixed apparent surface tension (Eq. 13), that is independent of tether length.

Bending and tension

The tether force at zero velocity is 8.2 pN (Fig. 5 *a*), and the tether radius is 210 nm, or 0.21 μm. Thus, from Eq. 27b, the bending modulus is

$$B = \frac{f_0 R_t}{2\pi} = 0.27 \text{ pN} \cdot \mu\text{m} = 2.7 \times 10^{-19} \text{ N} \cdot \text{m}.$$

The bending modulus for tethers extracted from SOPC vesicles is 1.1×10^{-19} N · m (Waugh et al., 1992; Yeung, 1994), that for SOPC/CHOL (1:1) is 2.2×10^{-19} N · m (Yeung, 1994), 2.5×10^{-19} N · m (Evans and Rawicz, 1990), or 3.3×10^{-19} N · m (Song and Waugh, 1993), and that for SM/CHOL (1:1) is 5.5×10^{-19} N · m (Yeung, 1994).

Now, Eq. 13, or Eq. 27c or 27d, can be used to calculate the apparent surface tension in neuronal growth cone membrane:

$$T + \gamma = \frac{f_0}{4\pi R_t} = 3.1 \text{ pN}/\mu\text{m} = 0.0031 \text{ mN/m(dyn/cm)}.$$

This is an extraordinarily small value for the apparent surface tension and accounts for the fact that the tether diameter is so large. Human neutrophils have a cortical tension that is ~10 times this value (Evans and Kukan, 1984; Needham and Hochmuth, 1992), and the membrane tension that is imposed on vesicles from which tethers are extracted is usually approximately 30–100 times larger than this value. The energy of association measured when tethers are extracted from red cells (Waugh and Bauserman, 1995) is ~2 orders of magnitude larger than this value.

The effect of various chemical treatments on the values of the apparent surface tension and the bending modulus is shown in Fig. 7, and the statistical significance of the difference in these values is given in Table 1. These calculations were performed by measuring the tether force at zero velocity and the tether radius and using Eqs. 27b and 27c as shown above.

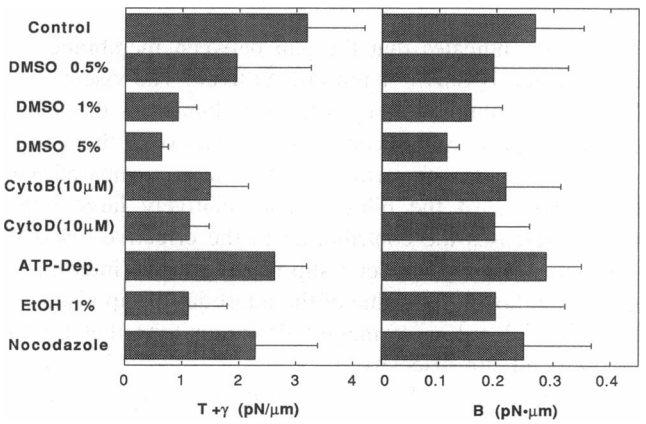

FIGURE 7 Effect of different chemical treatments on the apparent surface tension $T + \gamma$ and bending modulus B for the membrane of neuronal growth cones. The error bars for B and $T + \gamma$ stand for their standard errors of estimate (Spiegel, 1988). They were obtained with a statistical analysis, in which the standard error of estimate for f_0 and the standard deviation for R_t were used. DMSO, dimethylsurfoxide; CytoB, cytochalasin B; CytoD, cytochalasin D; ATP-Dep., ATP depletion; EtOH, ethanol. For detailed information on the treatments, refer to Dai and Sheetz (1995a).

Viscous drag and the "effective" viscosity

Because the tether radius remains constant, the viscous terms in Eq. 26 can be replaced by a single effective surface viscosity η_{eff}:

$$\eta_{eff} \equiv 2\eta_m + \eta_{si}h^2 \ln(R_o/R_t) + \eta_{sc}R_t^2 \ln(R_o/R_t). \quad (28)$$

Using the simplifications given by Eqs. 27a and 28 and neglecting the induced bending term and the $\pi h\gamma$ term allow Eq. 26 to be written as

$$f = f_0 + 2\pi\eta_{eff}V_t, \quad (29a)$$

where f_0 is given by Eq. 27 and η_{eff} is given by Eq. 28. Results such as those shown in Fig. 5 can be used to determine a value for η_{eff} according to

$$\eta_{eff} = \frac{f - f_0}{2\pi V_t}. \quad (29b)$$

For neuronal growth cones (Fig. 5), $\eta_{eff} = 0.137$ pN · s/μm. Values for η_{eff} obtained from the data of Evans and Yeung (1994) and Yeung (1994) (see Fig. 5 *b*) are, in units of pN · s/μm, 0.071 (SM/CHOL), 0.012 (SOPC/CHOL, estimated), and 0.009 (SOPC). (All values are at room temperature. Note that 1 pN · s/μm = 10^{-3} pN · s/nm = 10^{-3} dyn·s/cm.) Lipid membrane is thought to have a surface viscosity of $\sim 10^{-6}$ dyn·s/cm = 0.001 pN · s/μm (Evans and Yeung, 1994), so the contribution of the membrane viscos-

TABLE 1 Statistical significance of the changes in the properties of treated neuronal growth cones

Treatments	$T + \gamma$	B	η_{eff}
DMSO 0.5%	$p < 0.001$	$p < 0.01$	$p > 0.1$
DMSO 1%	$p < 0.001$	$p < 0.001$	$p < 0.01$
DMSO 5%	$p < 0.001$	$p < 0.001$	$p < 0.001$
Cytochalasin B	$p < 0.001$	$p > 0.1$	$p > 0.5$
Cytochalasin D	$p < 0.001$	$p > 0.01$	$p > 0.5$
ATP depletion	$p > 0.05$	$p > 0.5$	$p < 0.001$
Ethanol	$p < 0.001$	$p > 0.01$	$p > 0.5$
Nocodazole	$p < 0.01$	$p > 0.5$	$p > 0.1$

The p-values listed here were obtained by using the two-tailed t test for two heteroscedastic samples. The hypothesis is that $T + \gamma$, B, and η_{eff} are equal to their corresponding control values. For the measurement of the apparent surface tension all but the experiments involving ATP depletion are different from the control. For the measurement of the bending modulus, only the treatment with DMSO resulted in a significant difference. For the measurement of the effective viscosity, only ATP depletion and DMSO addition (at the two higher values) resulted in a significant difference.

ity to the effective viscosity in Eq. 28 is $2\eta_m = 0.002$ pN · s/μm. The question now is: Which viscous term in Eq. 28 makes the greatest contribution to the experimental measurement of the effective viscosity?

Interbilayer slip

This question is the easiest to answer for simple vesicles because here the term for cytoskeletal slip is zero. Also, the question must be answered for vesicles before it is possible to make conclusions about the main source of viscous resistance when membrane tethers are extracted from neuronal growth cones. For the vesicles studied by Evans and Yeung (1994), the interbilayer slip viscosity term from Eq. 34, with η_{sc}, is

$$\begin{aligned}\eta_{si}h^2 \ln(R_c/R_t) &= \eta_{eff} - 2\eta_m \\ &= 0.009 - 0.002 = 0.007 \text{ pN} \cdot \text{s}/\mu\text{m (SOPC)}, \\ &= 0.012 - 0.002 = 0.010 \text{ pN} \cdot \text{s}/\mu\text{m (SOPC/CHOL)}, \\ &= 0.071 - 0.002 = 0.069 \text{ pN} \cdot \text{s}/\mu\text{m (SM/CHOL)}.\end{aligned} \tag{30}$$

These values account for the interbilayer drag. Yeung (1994) reports values for $\eta_{si}h^2$ with the assumption that $2\eta_m$ is negligible. However, the membrane surface viscosity does appear to be significant, at least for the case of SOPC. (For SOPC membrane, increasing the assumed value for the membrane surface viscosity by a factor of 3 would make the viscous resistance of the membrane twice as large as that caused by interbilayer slip.) Three-dimensional or "bulk" values for the interbilayer slip viscosity, $\eta_{si}h$, can be calculated because h is of the order of 4 nm (0.004 μm) and $\ln(R_o/R_t)$ is of the order of 5.4 (estimated from Yeung, 1994). Thus, the three-dimensional values for the slip viscosity are 0.32 pN · s/μm^2 (SOPC), 0.46 pN · s/μm^2 (SOPC/CHOL) and 3.2 pN · s/μm^2 (SM/CHOL). At room temperature, common oils such as olive and castor oils have a viscosity between 0.5 and 5 P (dyn·s/cm^2), which is between 0.05 and 0.5 pN · s/μm^2. Therefore, the interbilayer slip viscosity for these simple vesicles has an equivalent, three-dimensional (bulk) value that is comparable with or somewhat larger than that for common oils.

Cytoskeletal slip

It is assumed that the simple membrane system that is closest to the membrane of neuronal growth cones is SOPC/CHOL. Neuronal growth cone membrane is saturated with cholesterol at nearly a 1:1 ratio, and the membrane consists of phospholipids with chain lengths similar to those of SOPC and with negligible amounts of sphingomyelin (Gennis, 1989). In addition, the bending moduli for the two membranes are similar. For SOPC/CHOL, Yeung (1994) gives a value for the interbilayer slip viscosity times the square of the membrane thickness. However, this value is based on the assumption that the membrane viscosity is negligible. From Eq. 30, it appears that neglecting the membrane viscosity gives an overestimate of ~20% in the value for the interbilayer slip viscosity. Thus the "corrected" value for the interbilayer slip is $\sim 20 \times 10^{-3}$ pN · s/μm. Now, when Eq. 28 is solved for the cytoskeletal slip term and this new slightly modified or "corrected" value for the membrane slip viscosity is substituted into the result, the following value for the cytoskeletal slip viscosity term is obtained:

$$\begin{aligned}&\eta_{sc}R_t^2 \ln(R_o/R_t) = \eta_{eff} - [2\eta_m + \eta_{si}h^2 \ln(R_o/R_t)], \\ &\eta_{sc}R_t^2 \ln(R_o/R_t) \\ &\quad = 0.137 - [0.002 + 0.002 \ln(R_o/R_t)] \text{ (pN} \cdot \text{s}/\mu\text{m)}.\end{aligned} \tag{31a}$$

For neuronal growth cones with disklike diameters of 10 μm, which gives an equivalent sphere radius of 3.54 μm, and for a tether radius of 0.21 μm, $\ln(R_o/R_t) = 2.82$. For these values of cell and tether radii, Eq. 31a becomes

$$\begin{aligned}\eta_{sc}R_t^2 \ln(R_o/R_t) &= 0.129 \text{ pN} \cdot \text{s}/\mu\text{m}, \\ \eta_{sc} &= 1.0 \text{ pN} \cdot \text{s}/\mu\text{m}^3.\end{aligned} \tag{31b}$$

It is postulated that this slip viscosity is due to a thin layer of water between the inner bilayer membrane and the cytoskeleton (Fig. 4 *a*). The mean or "effective" gap thickness of this putative layer can be obtained by dividing the viscosity of water at room temperature, which is ~0.01 dyn·s/cm^2 = 0.001 pN · s/μm^2, by the value for the slip viscosity given in Eq. 31b:

$$\begin{aligned}\eta_{sc}\delta = \eta_{water} \Rightarrow \delta &= \frac{\eta_{water}}{\eta_{sc}} = \frac{0.001 \text{ pN} \cdot \text{s}/\mu\text{m}^2}{1.0 \text{ pN} \cdot \text{s}/\mu\text{m}^3} \\ &= 0.001 \ \mu\text{m} = 1 \text{ nm}.\end{aligned} \tag{32}$$

The result indicates that the gap between membrane and cytoskeleton is only ~1 nm (10 Å) thick. The viscous slip between membrane and cytoskeleton dominates the tether-extraction processes because the gap between them is so small,~1 nm, and the tether radius is large compared with the thickness of the bilayer. The relatively large tether radius increases the contribution to the effective viscosity (Eq. 28) of the cytoskeletal slip relative to the interbilayer slip, even though the value of the interbilayer slip viscosity, [eta$_{si}$, is ~2 orders of magnitude larger than that for the cytoskeletal slip viscosity, η_{sc}.

Values for the effective viscosity for various chemical treatments of neuronal growth cones are shown in Fig. 8, and the significance of the change in values is shown in Table 1 (along with the significance of the change in values of the apparent surface tension and the bending modulus). In most cases the effective viscosity does not change significantly, which means, in accordance with the calculations given above, that the gap width between membrane and cytoskeleton does not change.

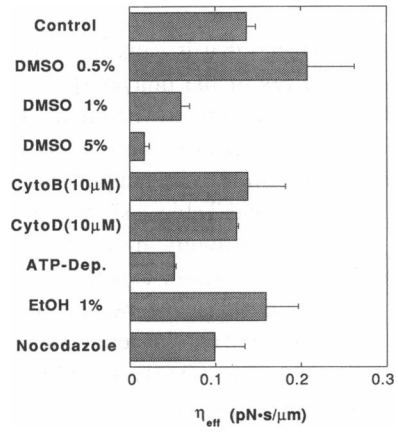

FIGURE 8 Effect of different chemical treatments on the effective viscosity for neuronal growth cone membrane as it flows from a growth cone into a tether; the error bars stand for the 68% confidence limits for η_{eff}. The treatments here are the same as those described in Fig. 7.

DISCUSSION

The theory developed in this paper is based on the simple geometry of a cylindrical tether drawn from a flat disk where the axis of symmetry of the tether is perpendicular to the plane of the disk as shown in Figs. 1–4. However, the neuronal growth cone is a disklike body that lies flat upon a surface as a tether is drawn from the edge of the disk (Dai and Sheetz, 1995a). It is possible mathematically to "map" two-dimensional, closed surfaces from one shape to another, say, from a prolate spheroid to a sphere to an oblate spheroid. In this manner the flat membrane disk with a tether extracted from its edge can be mapped into a axisymmetric disk with a tether being extracted along its axis of symmetry. Because of the mapping process, however, lines of constant velocity will not correspond to lines of constant radius, r, in Figs. 2–4. This will create flows and stresses in the angular (θ) direction, which will add some additional dissipation terms to the thermodynamic calculations based on Eqs. 14 and 15, although the mean velocity (obtained by integrating the velocity at a given r from θ equal 0 to 2π) will still vary as $1/r$ according to Eq. 16 because of conservation of mass. Now, because of this and because each of the viscous drag or dissipation terms depends on the square of the velocity (Eqs. 19, 21, and 24), it is suggested that although the coefficients that multiply the various viscous terms in Eq. 26 will change, the proportional relationship among these terms will not change. This, then, would not change the definition of effective viscosity given by Eq. 28. It would change only the value for the effective viscosity as calculated from Eq. 29b. Instead of a 2π term, there would be another, larger term. (The term would be larger because of the additional dissipation terms caused by the nonaxisymmetric flow in the θ direction.) But, even if the effective viscosity were to decrease by a factor of ~2, the cytoskeletal slip term as evaluated by Eq. 31a would still be significantly larger than the terms in this equation that account for the membrane viscosity and the interbilayer slip. Thus, the conclusion that the slip between the membrane and cytoskeleton dominates the flow process created by the extraction of a tether is still valid, although the estimate of the effective thickness of the lubricating film between membrane and cytoskeleton would increase by a factor of ~2 in this example.

The overall disklike shape of the cell was preserved and the axon remained extended during the various chemical treatments. It is important that chemical treatment not alter the shape of the growth cone in order that the measurements not reflect a juxtaposition of changes in both the extrinsic shape and the intrinsic material properties. A constant shape means that changes in the measured values of tether force and radius reflect a change in the intrinsic material properties of the membrane and its association with the cytoskeleton. Local changes did occur during the treatment with DMSO and the cytochalasins. These caused a loss of filopodia, which could be responsible for a reduction in the far-field component of the apparent tension by decreasing the intrinsic forces that push on the membrane.

Although the tether radius of a neuronal growth cone is large, its bending modulus is not. Its value of 2.7×10^{-19} N · m is comparable with values of 2.2×10^{-19}, 2.5×10^{-19}, and 3.3×10^{-19} N · m measured, respectively, by Yeung (1994), Evans and Rawicz (1990), and Song and Waugh (1993) for SOPC/CHOL. The reason that the tether radius is so large is that the apparent surface tension is so small, with a value calculated from Eq. 27c of ~0.003 mN/m. As mentioned above, this value is an order of magnitude smaller than the value for the cortical tension in neutrophils.

The bending modulus depends only on the composition and the structure of the membrane. Mathematically, $B = Kh^2/48$ (Waugh and Hochmuth, 1987), where K is the area expansion/compression modulus of the membrane. Thus, with a value of 4 nm for h we calculate a value for K of ~810 mN. Typical values for SOPC lipid bilayer membranes range from 100 to 500 mN/m (Bo and Waugh, 1989; Evans and Needham, 1987). The bending modulus does not appear to be affected significantly by any chemical treatment except for large concentrations of DMSO (Fig. 7 and Table 1). DMSO is a solvent and would readily dissolve in the lipid membrane, and it could thus change its bending modulus. Although ethanol is also a solvent, the concentration of ethanol used in the experiments does not seem to be large enough to change the bending modulus. The other chemical treatments are likely to affect the actin or microtubules of the cytoskeleton without affecting the lipid membrane.

Mathematically, it is impossible to separate the role of the in-plane, far-field tension T from that of the energy of adhesion γ. Only the sum of these two quantities can be calculated. In addition, although the "out and back" experiments show that the energy of adhesion is mechanically reversible, as described by Evans (1985), it is not clear whether the adhesion itself comes from some nonspecific association between membrane and cytoskeleton or from a

specific association caused by integral membrane proteins attached to the cytoskeleton. Schmidt et al. (1995) show that the β_1 integrins cause a strong coupling between the membrane and the cytoskeleton, especially at the leading edge of the growth cone where the actin is most organized. DMSO could weaken membrane–integrin associations, whereas the cytochalasins could weaken the association of the integrins with the cytoskeleton. Fig. 7 shows that this may be the case because both DMSO and the cytochalasins cause a significant reduction in the overall apparent surface tension. In addition to being a solvent, ethanol may alter the actin organization in cells (Weiss et al., 1991), and in this way it could decrease the apparent surface tension. Nocodazole has a slight effect on the apparent surface tension, probably by disrupting microtubules or intermediate filaments of neuronal growth cones (Wang et al., 1993). However, these chemical treatments could affect also the in-plane, far-field tension, and, unfortunately, there is no simple way to determine the separate roles of in-plane tension and adhesion because they appear together only as a sum. It is not surprising that ATP depletion does not change the apparent surface tension because it does not affect the membrane–cytoskeleton association (Dai and Sheetz, 1995a; Wang et al., 1993).

Tethers extracted from neuronal growth cones are significantly different from those extracted from red cells. Red cell tethers exhibit a hysteresis effect in that the "out" experiment is different from the "back" experiment (Hochmuth et al., 1982). Tethers from growth cones do not exhibit hysteresis. Tethers from red cells also exhibit, over several minutes, a long-term force relaxation when held at constant length (Hochmuth et al., 1973; Waugh and Bauserman, 1995), whereas tethers from neuronal growth cones and lipid vesicles do not. (When the tether is stopped suddenly, the tether force for vesicles and neuronal growth cones returns immediately to its zero-velocity value, while the tether radius does not change.) The "energy of association" measured by Waugh and Bauserman (1995) probably comes from the lateral segregation of lipids from integral membrane proteins as the lipids are drawn into the tether. The proteins "bunch up" in the neck of the tether when the tether is formed and disperse when the tether is allowed to retract. This could be responsible for the hysteresis effect in an "out" and "back" experiment. The energy measured by Waugh and Bauserman, 0.3 mN/m, is 2 orders of magnitude larger than the apparent surface tension (the sum of the far-field tension and the energy of adhesion) in the growth cone. For all these reasons, it is likely that the origins of the energy of adhesion in growth cones described here is different from that for the energy of association in red cells described by Waugh and Bauserman (1995).

For the first time, the viscous slip between membrane and cytoskeleton has been measured. The value for the slip viscosity is equivalent to the viscous resistance that would be created by a layer of water that is ~1 nm thick. The resistance caused by the slip of membrane over the cytoskeleton is shown to be the dominant viscous term when tethers are extracted from neuronal growth cones, in spite of the significant resistance that is caused by the viscous slip between the two halves of the bilayer (Evans and Yeung, 1994). It is the "amplification" by the relatively large tether radius (see Eq. 28) of the neuronal growth cone that causes the cytoskeletal slip term to be so important.

The results in Fig. 8 and Table 1 show that the value for the effective viscosity is strongly affected by large concentrations of DMSO and to a lesser extent by ATP depletion. Because the viscous resistance comes primarily from the slip between membrane and cytoskeleton and the slip occurs in a molecularly thin gap, simply doubling the spacing between membrane and cytoskeleton would halve the viscosity. It is interesting to note that in the case of DMSO both the viscosity and the apparent surface tension decrease together. Possibly, then, the energy of association γ is reduced, which results in an increase in the spacing between membrane and cytoskeleton and, therefore, in a lower value for the effective viscosity. However, the treatment with ATP results in a counter example in which there is a decrease in the effective surface viscosity with no significant change in the apparent surface tension. This is a surprising result for which we have no simple explanation.

The calculation of a value for cytoskeletal slip requires a value for the interbilayer slip and an estimate for the membrane viscosity. Evans and Yeung (1994) and Yeung (1994) give values for the interbilayer slip viscosity for different lipid bilayers. Even if their largest value for slip viscosity, that for SM/CHOL (Eq. 30), were used in the calculation of the cytoskeletal slip viscosity according to Eq. 31, the value for the cytoskeletal slip viscosity would be only ~20% less than the value given by Eq. 31b; i.e., $\eta_{sc} = 0.80$ pN · s/μm. This smaller value still indicates an extraordinarily small value of 1.25 nm (calculated from Eq. 32) for the effective thickness of the water film between membrane and cytoskeleton. In regard to the estimate for the membrane surface viscosity, even if this estimate were increased by an order of magnitude, it can be seen from Eq. 31a that this larger value for η_m would decrease the value for the cytoskeletal slip viscosity, η_{sc}, only by ~10%. Because of the extraordinarily large value for the effective viscosity and the large value for the tether radius when neuronal growth cone membrane is drawn into a tether, it can be stated that this process is dominated by the slip between membrane and cytoskeleton. This slip occurs in a thin film of water with an effective gap width, defined by Eq. 32, that is of the order of 1 nm. The conclusion that the flow process is dominated by the slip between membrane and cytoskeleton would still be true even if the values for the membrane surface viscosity and the interbilayer slip viscosity in Eq. 31a were increased by an order of magnitude. Even if biological surfaces are in intimate contact with each other and are separated only by atomic distances, they still can readily and rapidly slide over each other when acted on by forces on the order of a few piconewtons because of the wonderful lubricating properties of a thin film of water.

This work was supported by a National Institutes of Health grant (RO1 HL23728) to R.M.H. and grants from the National Institutes of Health, HFSP, and MDA to M.P.S.

REFERENCES

Bird, R. B., W. E. Stewart, and E. N. Lightfoot. 1960. Transport Phenomena. John Wiley & Sons Inc., New York.

Bo, L., and R. E. Waugh. 1989. Determination of bilayer membrane bending stiffness by tether formation from giant, thin-walled vesicles. *Biophys. J.* 55:509–517.

Dai, J., and M. P. Sheetz. 1995a. Mechanical properties of neuronal growth cone membranes studies by tether formation with laser optical tweezers. *Biophys. J.* 68:988–996.

Dai, J., and M. P. Sheetz. 1995b. Regulation of endocytosis, exocytosis and shape by membrane tension. *In* Protein Kenesis: Dynamics of Protein Trafficking and Stability. Coldspring Harbor Laboratory Press, New York. In press.

Evans, E. A. 1980. Minimum energy analysis of membrane deformation applied to pipet aspiration and surface adhesion of red blood cells. *Biophys. J.* 30:265–284.

Evans, E., and B. Kukan. 1984. Passive material behavior of granulocytes based on large deformation and recovery after deformation tests. *Blood.* 64:1028–1035.

Evans, E. A. 1985. Detailed mechanics of membrane-membrane adhesion and separation. *Biophys. J.* 48:175–183.

Evans, E. A., and D. Needham. 1987. Physical properties of surfactant bilayer membranes: thermal transitions, elasticity, rigidity, cohesion, and colloidal interactions. *J. Phys. Chem.* 91:4219–4228.

Evans, E., and W. Rawicz. 1990. Entropy-driven tension and bending elasticity in condensed-fluid membranes. *Phys. Rev. Lett.* 64: 2094–2097.

Evans, E., and A. Yeung. 1994. Hidden dynamics in rapid changes of bilayer shape. *Chem. Phys. Lipids.* 73:39–56.

Gelles, J., J. Schnapp, and M. P. Sheetz. 1988. Tracking kinesin-driven movements with nanometer-scale precision. *Nature (London.* 331: 450–453.

Gennis, R. B. 1989. Biomembranes. Springer-Verlag, Inc., New York.

Hochmuth, R. M., N. Mohandas, and P. L. Blackshear, Jr. 1973. Measurement of the elastic modulus for red cell membrane using a fluid mechanical technique. *Biophys. J.* 30:747–762.

Hochmuth, R. M., and E. A. Evans. 1978. Mechanochemical properties of membranes. *Curr. Top. Membr. Transp.* 10:1–64.

Hochmuth, R. M., and E. A. Evans. 1982. Extensional flow of erythrocyte membrane from cell body to elastic tether. I. Analysis. *Biophys. J.* 39:71–81.

Hochmuth, R. M., H. C. Wiles, E. A. Evans, and J. McCown. 1982. Extensional flow of erythrocyte membrane from cell body to elastic tether. II. Experiment. *Biophys. J.* 39:83–89.

Hochmuth, R. M., E. A. Evans, H. C. Wiles, and J. McCown. 1983. Mechanical measurement of red cell membrane thickness. *Science.* 220:101–102.

Kuo, S. C., and M. P. Sheetz. 1993. Force of single kinesin molecule measured with optical tweezers. *Science.* 260:232–234.

Needham, D., and R. M. Hochmuth. 1992. A sensitive measure of surface stress in the resting neutrophil. *Biophys. J.* 61:1664–1670.

Schmidt, C. E., J. Dai, D. A. Lauffenburger, M. P. Sheetz, and A. F. Horwitz. 1995. Integrin-cytoskeletal interactions in neuronal growth cones. *J. Neurosci.* 15:3400–3407.

Schnapp, B. J., J. Gelles, and M. P. Sheetz. 1988. Nanometer-scale measurements using video light microscope. *Cell Motil. Cytoskel.* 10:47–53.

Song, J., and R. E. Waugh. 1993. Bending rigidity of SOPC membrane containing cholesterol. *Biophys. J.* 64:1967–1970.

Spiegel, M. R. 1988. Schaum's Outline Series: Theory and Problems of Statistics. McGraw-Hill, Inc., New York.

Wang, N., J. P. Butler, and D. E. Ingber. 1993. Mechanotransduction across the cell surface and through the cytoskeleton. *Science.* 260: 1124–1127.

Waugh, R. E. 1982. Surface viscosity measurements from large bilayer vesicle tether formation. II. Experiments. *Biophys. J.* 38:29–37.

Waugh, R. E., and R. M. Hochmuth. 1987. Mechanical equilibrium of thick, hollow, liquid membrane cylinders. *Biophys. J.* 52:391–400.

Waugh, R. E., J. Song, S. Svetina, and B Žekš. 1992. Local and nonlocal curvature elasticity in bilayer membrane by tether formation from lecithin vesicles. *Biophys. J.* 61:974–982.

Waugh, R. E., and R. G. Bauserman. 1995. Physical measurements of bilayer-skeletal separation forces. *Ann. Biomed. Eng.* 23:308–321.

Waugh, R. E., and R. M. Hochmuth. 1995. Mechanics and deformability of hematocytes. *In* The Biomedical Engineering Handbook. J. D. Bronzino, editor. CRC Press, Inc., Boca Raton, FL. 474–486.

Weiss, L., B. B. Asch, and G. Elkin. 1991. Effects of cytoskeleton perturbation on the sensitivity of Ehrlich ascites tumor cell surface membranes to mechanical trauma. *Invas. Metast.* 11:93–101.

Yeung, A. 1994. Mechanics of inter-monolayer coupling in fluid surfactant bilayers. Ph.D. thesis. Department of Physics, University of British Columbia, Canada.